

1 **Global Nitrogen and Sulfur Deposition Mapping Using a**
2 **Measurement-Model Fusion Approach**

3 **Hannah J. Rubin¹, Joshua S. Fu^{1,2}, Frank Dentener³, Rui Li⁴, Kan Huang⁵, Hongbo Fu⁵**

4 ¹Department of Civil and Environmental Engineering, University of Tennessee, Knoxville, TN, 37996, USA

5 ²Computational Earth Science Group, Oak Ridge National Laboratory, Oak Ridge, TN 37831, USA

6 ³European Commission, Joint Research Centre, Sipra, Italy

7 ⁴Ministry of Education Key Laboratory for Earth System Modeling, Department of Earth System Science, Tsinghua
8 University, Beijing, 100084, China

9 ⁵Shanghai Key Laboratory of Atmospheric Particle Pollution and Prevention (LAP3), Department of Environmental
10 Science and Engineering, Fudan University, Shanghai, 200433, China

11 E-mail: jsfu@utk.edu

12 E-mail: jsfu@utk.edu
13
14 **Keywords:** Measurement-model fusion, nitrogen deposition, sulphur deposition, HTAP II,
15 ammonia, multiple-model mean

16

17 **Abstract**

18 Global reactive nitrogen (N) deposition has more than tripled since 1860 and is expected to
19 remain high due to food production and fossil fuel consumption. [Global sulfur emissions have](#)
20 [been decreasing worldwide over the last 30 years, but many regions are still experiencing](#)
21 [unhealthily high levels of deposition.](#) We update the 2010 global deposition budget for reactive
22 nitrogen and sulfur components with new regional wet deposition measurements from Asia,
23 improving the ensemble results of eleven global chemistry transport models from the second
24 phase of the United Nation’s Task Force on Hemispheric Transport of Air Pollution (HTAP-II).
25 The observationally adjusted global N deposition budget is 114.5 Tg-N, representing a minor
26 increase of 1 % from the model-only derived values, and the adjusted global sulfur deposition
27 budget is 88.9 Tg-S, representing a 6.5% increase from the modelled values, using an
28 interpolation distance of 2.5 degrees. Regionally, deposition adjustments can be up to ~73% for
29 nitrogen, and 112% for sulfur. Our study demonstrates that a global measurement-model fusion
30 approach can improve N and S deposition model estimates at a regional scale, with sufficient
31 availability of observations, but in large parts of the world, alternative approaches need to be
32 explored. The analysis presented here represents a step forward toward the World
33 Meteorological Organization’s goal of global fusion products for accurately mapping harmful air
34 pollution deposition.

35

36 **1. Introduction**

37 Atmospheric nitrogen and sulfur deposition from human activities related to the use of fossils
38 and land use have significant implications for ecosystem and human health. Elevated levels of
39 nitrogen and sulfur can lead to eutrophication (Anderson et al., 2008; Heisler et al., 2008),
40 changes in carbon sequestration (Kicklighter et al., 2019; de Vries et al., 2009; Zhu et al., 2020),
41 loss of biodiversity (Clark et al., 2013; Dise and Stevens, 2005), and acidification (Bowman et
42 al., 2008). While sulfur deposition is expected to decrease over the next 80 years (Lamarque et
43 al., 2013), it will remain a serious hazard in many emerging economies. For instance, sulfur
44 deposition in East Asia peaked in 2006 (Lu et al., 2010) but is still high enough to be concerning,
45 especially in natural and semi-natural regions (Doney et al., 2007; Luo et al., 2014).

Deleted: ¶

47 Oxidized nitrogen (NO_x) and reduced nitrogen (NH_x), together called reactive nitrogen (Nr), and
48 oxidized sulfur (SO_x) deposition occur as wet and dry processes (Dentener et al., 2006). Wet
49 deposition is measured at hundreds of locations in Europe, North America, and Asia, but dry
50 deposition is harder to measure and is often instead derived from ambient concentrations and
51 modeled deposition velocities (Xu et al., 2015). For example, dry deposition is inferred from
52 continuous concentration measurements combined with modeled dry deposition velocities at a
53 few locations in North America (Clean Air Status and Trends Network (CASTNET), 2021) and
54 Asia (Acid Deposition Monitoring Network in East Asia (EANET), 2021).

55 The United Nations Economic Commission for Europe's Task Force on Hemispheric Transport
56 of Air Pollution (HTAP) is an international effort to improve the understanding of air pollution
57 transport science with emissions models. The second phase of HTAP was launched in 2012. Tan
58 et al. (2018) used the multi-model mean (MMM) of 11 HTAP II chemistry transport models to
59 estimate the sulfur and nitrogen deposition budgets for 2010. Significant uncertainty remained
60 due to a lack of station measurements, especially in East Asia, a large contributor to the overall
61 budget. Tan et al. (2018) compared Acid Deposition Monitoring Network in East Asia (EANET
62 (Acid Deposition Monitoring Network in East Asia, 2021)) measurements to the MMM output
63 but there were very few measurements in East Asia and all were located along the southeastern
64 coast. In contrast, the highest emissions and modeled deposition were inland and north, making it
65 challenging to evaluate model performance.

66 Combining measurements and model estimates in a "measurement-model fusion" (MMF)
67 approach has the advantage of retaining the broad spatial coverage of models while accurately
68 matching observations. Generally speaking, MMF takes model estimates of concentrations or
69 fluxes for a region and modifies them based on in-situ point measurements to force the model
70 towards the observed values (Labrador et al., 2020). One global MMF approach for wet
71 deposition combined measurements with HTAP I ensemble model values for 2000-2002 (Vet et
72 al., 2014) where model estimates filled empty grid cells lacking a 3-year observed mean.
73 Another MMF approach in North America (Atmospheric Deposition Analysis Generated from
74 optimal Interpolation from Observations, "ADAGIO") used observed concentrations to adjust
75 predicted concentrations from the Global Environmental Multiscale-Modelling Air Quality and
76 Chemistry (GEM-MACH) model (Schwede et al., 2019). Recent work in the US (Schwede and
77 Lear, 2014; Zhang et al., 2019) incorporates Community Multiscale Air Quality (CMAQ) model

Deleted: os

79 output and precipitation data generated by the Parameter-elevation Regressions on Independent
80 Slopes Model (PRISM, <https://prism.oregonstate.edu/>, Accessed: 10/01/22), as well as
81 observations using inverse distance weighting to create total deposition (“TDep”,
82 <https://nadp.slh.wisc.edu/committees/tdep/#tdep-maps>) maps that are publicly available.
83 More details of the MMF approach are described in Fu et al. (2022) as they lay out a roadmap
84 for future work, following the World Meteorological Organization’s Global Atmosphere Watch
85 Program (WMO GAW) and the intended role of the MMF Global Total Atmospheric Deposition
86 (MMF-GTAD) project. This study updates Tan et al.’s (2018) global S and N deposition
87 budgets using a variation of the TDep methodology (Schwede and Lear, 2014) to merge NH_x,
88 NO_y, and SO_x modelled gridded deposition fluxes results with deposition fluxes derived from
89 observations of NO₃⁻, NH₄⁺, and SO₄²⁻ in precipitation and precipitation amounts The main
90 purpose of our study is to demonstrate the viability of a straightforward but globally applicable
91 MMF approach, while remaining consistent with previous work that provided datasets for impact
92 assessments for various communities. This approach is an important intermediate step towards
93 the WMO’s goal of reliable deposition products to aid decision-making. We update the 2010
94 deposition budgets using MMF to combine the broad spatial coverage of a model with accurate
95 in-situ measurements.

96 2. Data Availability

97 **Table 1:** Sources of deposition observations.

Name	Source	Number of Observation Sites	Region	Value
NTN, AIRMoN	NADP	247	USA	wet deposition
CASTNET	NADP	84	USA	dry deposition
CAPMoN	NAChem	27	Canada	wet and dry deposition
EMEP	EMEP	86	Europe	wet deposition
China Scientific Study	Li et al. 2019	407	China	wet deposition

Deleted: s

EANET	EANET	47	East Asia	wet and dry deposition
IDAF	INDAAF	1	Niger	wet deposition

99

100 All data are from 2010, reported monthly with sources summarized in Table 1. Wet deposition
101 measurements (NO_3^- , NH_4^+ , and SO_4^{2-}) from the US's National Trends Network (NTN) and
102 Atmospheric Integrated Research Monitoring Network (AIRMoN) are available through the
103 National Atmospheric Deposition Program (NADP (National Atmospheric Deposition Program,
104 2021), <http://nadp.slh.wisc.edu/NTN/>). Measurements were filtered for completeness and quality,
105 following Schwede and Lear (2014). Sites without a full year of measurements or with quality
106 tags indicating collection issues were not included, resulting in 247 observations in the US. Dry
107 deposition generated values are available from the Clean Air Status and Trends Network
108 (CASTNET, 2021) at 84 locations. CASTNET uses an inferential method to calculate dry
109 deposition fluxes as a product of surface concentration and modeled dry deposition velocity.
110 Nitrogen and sulfur wet deposition measurements and dry deposition estimates throughout
111 Canada are recorded by the Canadian Air and Precipitation Monitoring Network (CAPMoN
112 (2021) and are available through the National Atmospheric Chemistry (NAtChem) database
113 (<https://donnees.ec.gc.ca/data/air/monitor/>). Dry deposition estimates from CAPMoN are
114 calculated by multiplying atmospheric concentration and deposition velocity. There were 27 sites
115 with a full year of quality checked data for 2010.
116 The European Monitoring and Evaluation Programme (EMEP (European Monitoring and
117 Evaluation Programme (EMEP), 2021; Tørseth et al., 2012), <http://ebas-data.nilu.no/>) provides
118 records of precipitation chemistry (NO_3^- , NH_4^+ , and SO_4^{2-}) and precipitation depths for Europe.
119 There were 86 sites with a full year of quality checked data in 2010.
120 In China, a multi-year nationwide field study, including some of these NNDMN data, was
121 compiled by Li et al. (2019). Daily NO_3^- , NH_4^+ , and SO_4^{2-} site measurements (in mg/L) were
122 averaged for 2010 for each of the 407 site locations with complete records by multiplying the
123 concentration by the precipitation recorded at that same site (in mm) and then aggregating to
124 produce annual precipitation-weighted deposition (Sirois, 1990). For a wider Asian region,

125 EANET (Asia Center for Air Pollution Research, 2021, <https://www.eanet.asia/>) wet and dry
126 deposition and precipitation data are available at 47 sites.

127 The International Global Atmospheric Chemistry (IGAC) Deposition of Biogeochemically
128 Important Trace Species (DEBITS) Africa (IDAF) program (Adon et al., 2010; Galy-Lacaux et
129 al., 2014) has NH₄⁺ and NO₃⁻ precipitation concentrations on the International Network to Study
130 Deposition and Atmospheric Chemistry in Africa (INDAAF (INDAAF – International Network
131 to study Deposition and Atmospheric chemistry in Africa, 2021)) website ([https://indaaf.obs-
133 mip.fr/](https://indaaf.obs-
132 mip.fr/)) for one site in Niger. All measurements were converted to mg-N (or S) /m²/yr.

Deleted: ¶

Formatted: Space After: 0 pt

134 3. Measurement Model Fusion Procedure

135 Global yearly wet and dry NO₃⁻, NH₄⁺, and SO₄²⁻ deposition observations (for wet deposition) or
136 estimates derived from near-surface concentrations and modelled deposition velocities for dry
137 deposition) were combined with the respective HTAP II model average grid cell estimates, using
138 model output interpolated to common 1 degree x 1 degree (1° x 1°) grid cells (Figure 1). For
139 example, wet NO₃⁻ deposition observations are combined with the wet NO₃⁻ modeled deposition
140 in the nearest HTAP II MMM grid cell to the observation, where observations exist. Dry
141 deposition values (NO₃⁻, NH₄⁺, and SO₄²⁻) from CASTNET and an inverse-distance weighted 1°
142 x 1° gridded dataset was created based on the distance from each observation to the center of the
143 nearest HTAP II model grid cell. Inverse-distance weighting (IDW) was selected as the most
144 straight forward to implement method to introduce MMF on a global scale while remaining
145 consistent with previous work (Schwede and Lear, 2014).

146 The weighting function was calculated as

$$147 \left(1 - \frac{\text{distance}}{\text{max distance}}\right)^2 \quad (1)$$

148 following Schwede and Lear's (Schwede and Lear, 2014) approach for the TDep product, where
149 "distance" is the distance between the site location and the center of the HTAP II model grid cell
150 nearest to that sampling site location, within a maximum distance of 2.5° (approximately 280 km
151 at middle latitudes). The choice of the maximum distance is a crucial parameter for the inverse
152 distance weighting method in MMF. Prior analysis (e.g. Tan et al. 2018b) has shown that
153 gaseous and particulate sulfur and nitrogen emissions can travel several hundreds of kilometers,

155 before being deposited, although there is likely to be a large variation of transport distances due
156 to regional differences in chemistry, meteorological conditions, transport patterns and removal
157 processes. These processes interact with spatially heterogeneous emissions. Since there will not
158 be a single distance that captures the heterogeneity of all processes at play, we present here a
159 base case using a 2.5° interpolation distance, and two sensitivity cases reducing the distance to 1°
160 and increasing it to 5°, respectively. The 5° distance can be seen as an upper limit for the distance
161 where deposition observations can constrain deposition. The output values of the weighting
162 function at each observation location are then multiplied by the observed deposition. For the
163 center of every HTAP II model grid cell near that site, the modeled deposition is multiplied by 1
164 minus the value of the weighting function. Consequently, if there are no observations near the
165 model grid cells, the cell value remains the same. The two grid values ([weighting function times
166 observed deposition] and [1-weighting function times modeled deposition]) are added together to
167 give the value of the MMF estimate. This has the effect of modifying the HTAP II grid values
168 only in locations where there are observations within the maximum interpolation distance.

169 The MMF gridded surfaces were then summed by species along with the remaining unchanged
170 HTAP II gridded surfaces that lacked in-situ measurements to create total N and S deposition
171 gridded surfaces (e.g., the MMF wet and dry SO₄⁻ gridded surfaces were added to the HTAP II
172 wet and dry SO₂ gridded surfaces to get total S deposition). The MMF wet deposition surfaces
173 include measurements from Europe, Asia, and North America, and the dry deposition MMF
174 surfaces include estimates from the USA and Asia (see section 2)

175

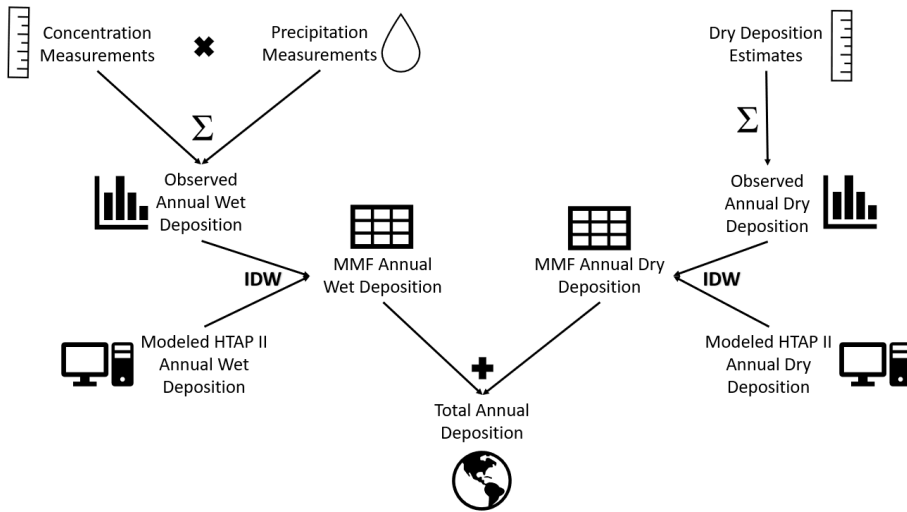


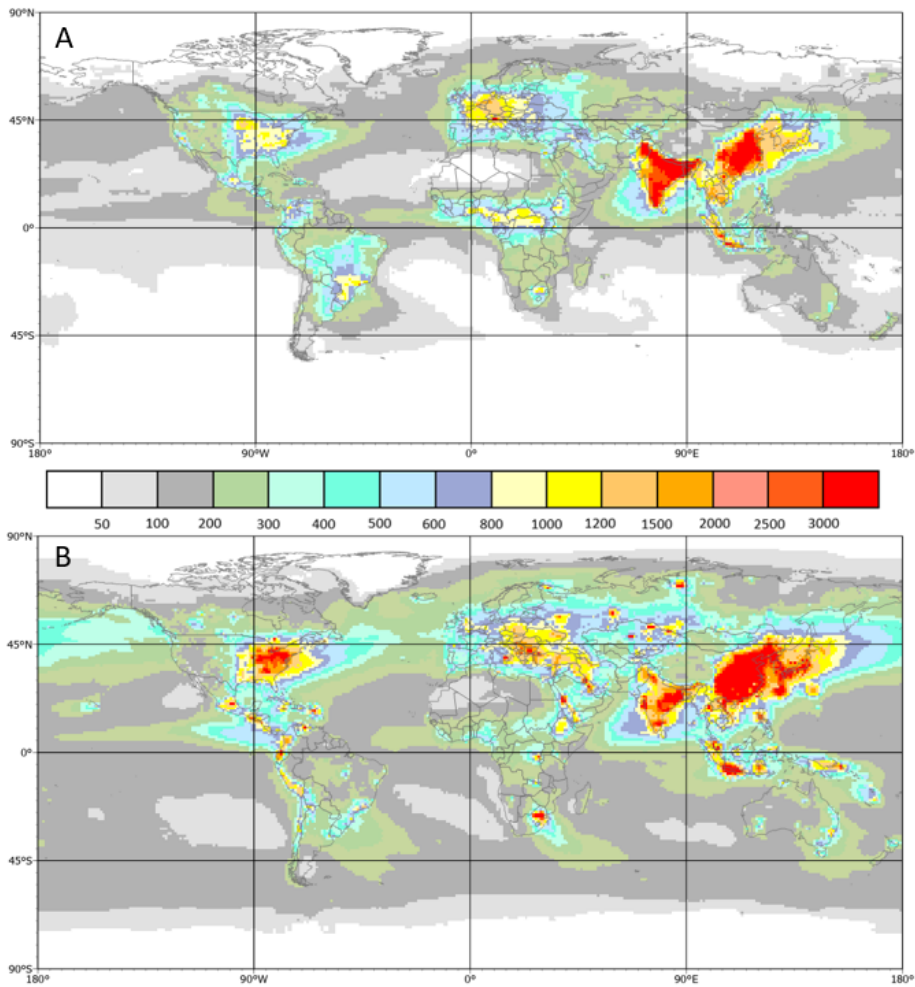
Figure 1. A flowchart describes the MMF methodology implemented in this paper.

4. Results

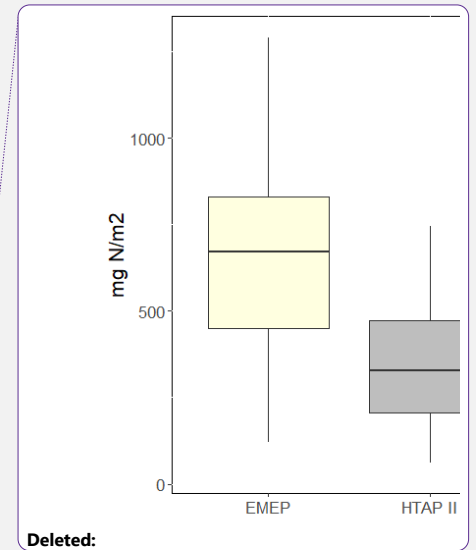
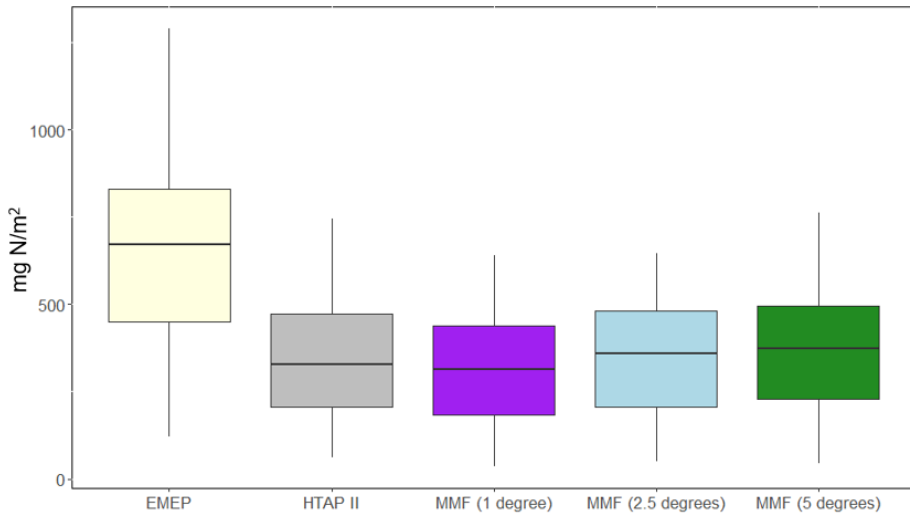
The total global NH_x deposition in 2010 increased from 54.0 Tg-N (from HTAP II models) to 54.9 Tg-N (Table 2). Combined with a NO_y deposition of 59.6 Tg-N (from a modeled HTAP II 59.3 Tg-N), the total global deposition is adjusted to 114.5Tg-N (from 113 Tg-N), an increase by 1 %. While the IDW tends to decrease the depositions over the continents, an increase is calculated over coastal regions and open oceans using the 2.5x2.5 maximum distance. Total S deposition is adjusted to 88.91 Tg-S (Table 2), an increase by 6.5 % from the HTAP II model prediction of 83.5 Tg-S (Figure 2B). Regional changes greater than or equal to 10% are bolded and italicized.

Table 2: 2010 adjusted global wet and dry deposition in Tg N or Tg S. MMM indicates Tan et al.'s 2018 multi-model mean and MMF is this measurement-model fusion work with a 2.5° interpolation distance. [The 1° and 5° interpolation distance results are shown in Tables S1 and S2.](#) Coastal means deposition on sea within 1 degree of the coastline. RBU is an abbreviation for Russia, Belarus, and Ukraine. Open ocean does not include near-land “coastal” waters. The regions can be seen in the world map in Figure S1. Regional changes greater than or equal to 10% are bolded and italicized.

	Non-Coastal		Coastal		Non-Coastal		Coastal		Non-Coastal		Coastal	
	MMM	MMF	MMM	MMF	MMM	MMF	MMM	MMF	MMM	MMF	MMM	MMF
Region	Total NH _x				Total NO _y				Total SO _x			
North America	3.40	3.66	0.40	0.31	4.40	4.50	0.80	0.94	4.70	5.67	1.30	1.69
Europe	2.50	2.68	0.80	1.14	2.60	2.42	1.20	1.75	2.70	2.50	1.50	3.18
South Asia	8.60	8.60	1.00	1.00	3.60	3.60	0.70	0.70	3.70	3.70	1.00	1.00
East Asia	6.70	6.49	1.00	1.04	8.30	6.90	2.20	2.45	11.20	11.89	2.90	4.10
Southeast Asia	3.20	2.22	1.60	2.12	1.90	1.60	1.40	1.44	2.40	0.81	2.80	0.56
Australia	0.40	0.40	0.40	0.40	0.60	0.60	0.40	0.40	1.00	1.00	1.50	1.50
North Africa	0.70	0.70	0.20	0.20	1.40	1.40	0.40	0.40	1.00	1.00	0.50	0.50
Sub-Saharan Africa	3.40	3.40	0.40	0.40	4.70	4.70	0.60	0.60	2.70	2.70	0.70	0.70
Middle East	0.50	0.38	0.10	0.10	1.40	1.31	0.30	0.30	1.70	3.18	0.60	0.60
Central America	1.40	1.40	0.60	0.60	1.20	1.20	0.80	0.80	1.40	1.40	1.40	1.40
South America	3.80	3.80	0.30	0.30	3.40	3.40	0.30	0.30	2.40	2.40	0.60	0.60
RBU	1.80	1.18	0.30	0.08	2.40	1.36	0.50	0.47	3.60	5.10	0.90	1.17
Central Asia	0.50	0.32	0.00	0.00	0.60	0.55	0.00	0.00	1.20	1.88	0.10	0.10
Antarctica	0.10	0.10	0.00	0.00	0.10	0.10	0.00	0.00	1.40	1.40	0.00	0.00
Continental	37.00	35.33	7.10	7.69	36.70	33.64	9.70	10.55	41.00	44.63	15.60	17.10
Open Oceans	9.90	11.86			12.90	15.43			26.90	27.18		
Global	46.90	47.19	7.10	7.69	49.60	49.07	9.70	10.55	67.90	71.81	15.60	17.10



196
 197 **Figure 2: Total N and S deposition in 2010 using the MMF approach. A)** Total annual N deposition (mg N/m²),
 198 the sum of wet and dry NO₃⁻ and NH₄⁺ after applying the MMF approach, as well as HTAP II gridded surfaces of
 199 dry deposition of NH₃, HNO₃, and NO₂ with no MMF adjustment due to the lack of measurements. **B)** Total S
 200 deposition (mg S /m²), the sum of wet and dry MMF SO₄²⁻ and wet and dry HTAP II SO₂.

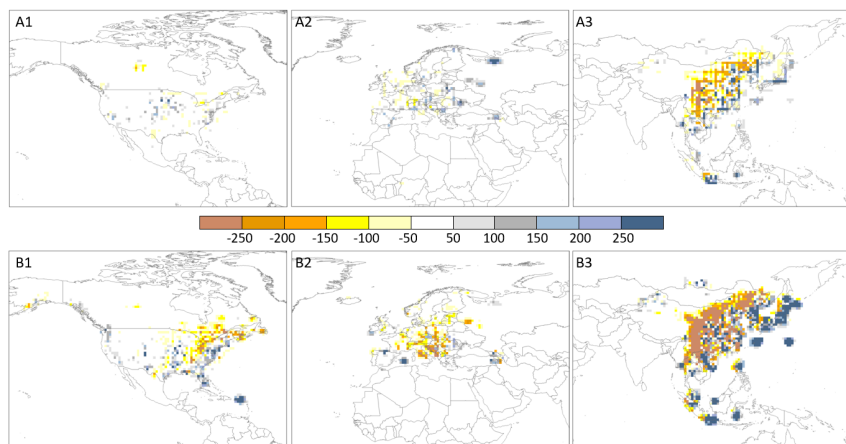


Deleted:

201
 202 **Figure 3: A comparison between HTAP II, MMF, and EMEP wet deposition fluxes in Europe results at**
 203 **EMEP observation sites.** A boxplot shows the distribution of EMEP, HTAP II, and MMF modeled wet reactive
 204 nitrogen deposition (NH_x and NO_y) results at each EMEP observation location. Three different interpolation
 205 distances are compared using MMF, 1 degree, 2.5 degrees, and 5 degrees.

206 Tan et al. (2018) report that their MMM underestimates the high observations of total N
 207 deposition at some EMEP stations in Europe. We find that our 2.5° interpolation value for
 208 European wet N deposition (8.0 Tg) is increased by 12.5% relative to the MMM surface (7.1
 209 Tg), although the distance to the observations remains high (Figure 3). Figures 4, S4 and S5
 210 show the difference between HTAP-II MMM and MMF nitrogen and sulfur deposition in North
 211 America, Europe, and Asia in mg/m^2 with different interpolation distances. As the interpolation
 212 distance increases, locations with a single measurement that is very different from the model will
 213 influence the surrounding grid cells to be higher than the model. This effect is in particular
 214 pronounced for sulfur deposition in Southeast Asia (Figure 4 B3) where the MMF procedure
 215 increases deposition by up to $250 \text{ mg}/\text{m}^2$ relative to the MMM values.

216



218

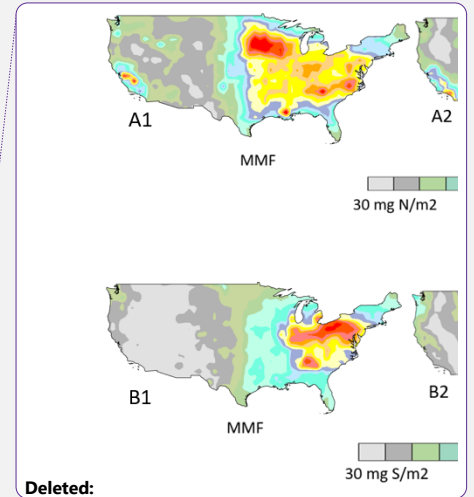
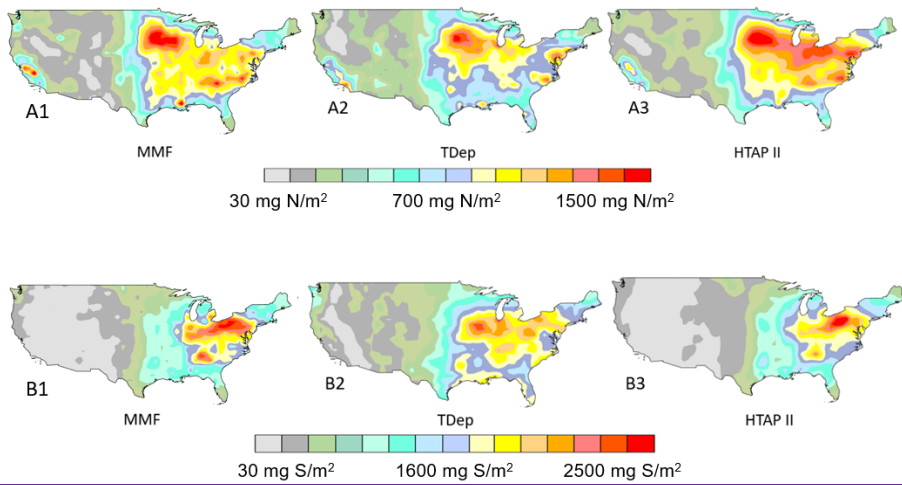
219 **Figure 4. The difference between MMF and MMM deposition with a 2.5-degree interpolation distance. A)**
 220 **MMF minus MMM reactive nitrogen deposition in North America (A1) Europe (A2) and East Asia (A3) in mg**
 221 **N/m^2 . B) MMF minus MMM sulfate deposition in North America (B1) Europe (B2) and East Asia (B3) in mg**
 222 **S/m^2 .** Results for other interpolation distances are shown in Figures S4 and S5, respectively.

223

224 The spatial distribution is slightly different, with more deposition in coastal areas in the MMF
 225 estimate (Table 2). Tan et al. (2018) report that the HTAP II MMM overestimates NO_3^- wet
 226 deposition in North America, but underestimates NH_4^+ deposition. We find that the MMF
 227 interpolated deposition slightly improves these estimates, although the spatial distribution is very
 228 similar with the MMM (Figures 2, 5). The largest change for S deposition (comparing MMM
 229 and MMF) is in grid cells classified as ocean because of an increase in East and Southeast Asia
 230 deposition which mostly occurs in areas classified as ocean due to the small island size relative
 231 to the coarse spatial resolution of the models. We note that, ocean cells were classified as such if
 232 they were located further than 1° from the mainland; therefore, any islands smaller than 1°
 233 were counted as the ocean.

234

235



236

237 **Figure 5: 2010 Total N deposition in the continental USA. A)** Total N is modeled with 1) MMF (this work), 2)
 238 TDep annual map available from the NADP and 3) Tan et al.'s 2018 MMM. **B)** 2010 SO_x wet deposition in the US
 239 as modeled with 1) MMF (this work), 2) TDep annual map available from the NADP, and 3) Tan et al.'s 2018
 240 multi-model mean HTAP II output.

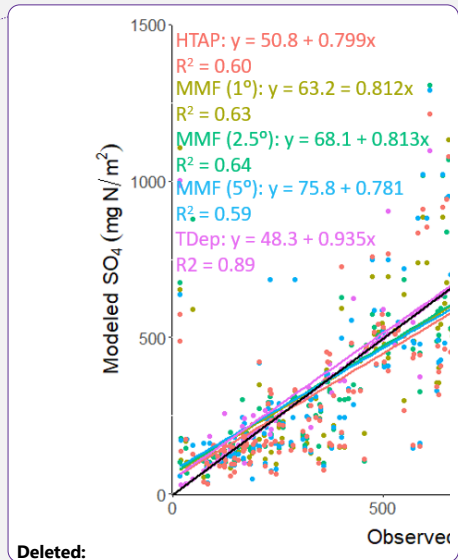
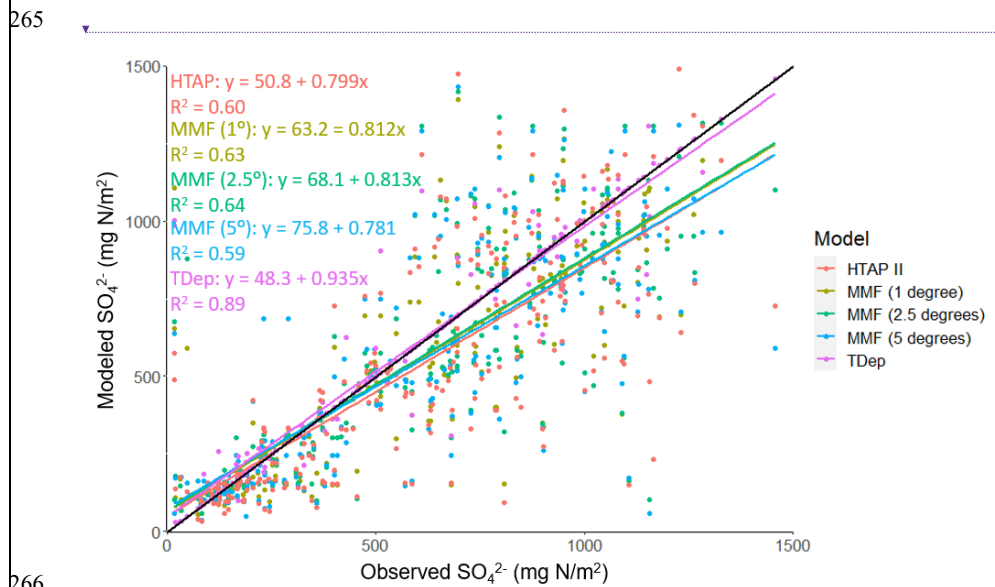
241

242 There are spatial differences between an aggregated 1° x 1° version of the original TDep map of
 243 nitrogen deposition for the United States as available from the NADP (Figure 5A2), the HTAP II
 244 (Figure 5A3) deposition produced by Tan et al. (2018) corresponding to the same area, and the
 245 deposition map produced in this work (Figure 5A1). A similar pattern is seen in the map of SO₄²⁻
 246 deposition (Figure 5B1; 5B3; 5B3). While the TDep maps have been aggregated to the 1x1
 247 degree resolution of the HTAP fields, there is still different regional variation in the deposition
 248 patterns in the TDep maps than the HTAP II maps. In particular, TDep is capturing higher west
 249 coast values that HTAP II does not while showing lower values in the Midwest/New
 250 York/Pennsylvania region.

251 The R² value for the linear regression between MMF wet SO₄²⁻ and observed wet SO₄²⁻ in the US
 252 is 0.64 (Figure 6). The R² value for the linear regression between the HTAP II wet SO₄²⁻ and
 253 observed SO₄²⁻ is 0.0.60, and 0.89 for the linear regression between the TDep wet SO₄²⁻ and
 254 observed SO₄²⁻ (Figure 6). This means that TDep is better reproducing the NADP/NTN

256 measurements and their spatial differences, whereas the MMF fields remain more similar to the
 257 HTAP II ensemble model output. The higher TDep R² value likely occurs because of the finer
 258 mesh (12 km) used in the TDep product, the closer proximity to individual stations as compared
 259 to HTAP II used in the MMF approach, and the ability of the regional model to capture
 260 gradients. In principle, emissions should be the same but in global models they are averaged over
 261 larger areas. All three datasets produce similar values to the measured wet SO_x deposition at the
 262 NADP/NTN sites (Figure 6). The NH₄ and NO₃ wet deposition values are shown in Figures S2
 263 and S3, and have much lower correlations (for all three interpolation distances), with an R² of 0.1
 264 for NO₃ and 0.53 for NH₄ at a 2.5° weighted distance

Deleted: supplemental
 Deleted: f



Deleted:

267 **Figure 6: Observed and modeled wet SO₄²⁻ deposition in the US in 2010.** Each NADP/NTN wet deposition
 268 measurement and the associated HTAP II, TDep, or MMF NH_x wet deposition modeled value, with all values
 269 shown together in A. The black line is the 1:1 line. Similar plots are shown in Figures S2 and S3 for wet NO₃ and
 270 wet NH₄.

271
 272 **5. Discussion**

273 *5.1 Consistency of MMF deposition with global emission estimates.*

277 Geddes et al. (2017) used satellite observations to report global NO_y emissions of 57.5 Tg-N/yr
278 in 2010, similar to the 60.4 Tg-N emissions reported by HTAP II. This matches well with our
279 total global MMF-derived NO_y deposition (58.1 Tg-N). HTAP II ammonia emissions were 59.3
280 Tg-N, slightly lower than the MMF NH₃ and NH₄⁺ deposition of 62.3 Tg-N. The total MMM
281 sulfur emissions for 2010 were 90.7 Tg S, very similar to the MMF sulfur deposition of 88.9 Tg-
282 N.

283 5.2 Deposition over China.

284 A promising data set of wet deposition measurements (NO₃⁻, NH₄⁺, and SO₄²⁻) in China is
285 available through the National Nitrogen Deposition Monitoring Network (NNDMN (Xu et al.,
286 2019)). It is comparable to other regional measurements (Wen et al., 2020). However, these data
287 only exist for a fraction of 2010 (from September onwards) for a few sites; rather than use partial
288 data to represent an entire year, these sites were not included in our study. Research in China
289 (Liu et al., 2020) analyzed the spatial pattern of N deposition by combining satellite observations
290 with NNDMN deposition measurements (Xu et al., 2019); they found a 2012 average of 18.21 kg
291 N ha⁻¹ for China? Additional work combining the GEOS-Chem
292 (<http://acmg.seas.harvard.edu/geos/>) model with satellite observations and surface measurements
293 reports the average annual deposition from 2008-2012 as 16.4 Tg-N with 10.2 Tg-N from NH_x
294 and 6.2 Tg-N from NO_y (Zhao et al., 2017). The averages reported by these studies are consistent
295 with ours (16.9 kg ha⁻¹ yr⁻¹) despite the difference in year and spatial resolution. The spatial
296 pattern of N deposition in 2010 (Figure 2A) also remains similar to that of previous decades (Jia
297 et al., 2014), with high deposition in eastern China and low deposition over the Tibetan Plateau.
298 This pattern is confirmed in 2006 and 2013 (Qu et al., 2017).

299 5.3 Limitations of interpolation

300 As seen in Table 2, the largest difference between MMM and MMF is found in coastal regions
301 and particularly the open ocean. While MMF does give improved deposition estimates by
302 incorporating in-situ measurements, it is worth considering the scale of the model. Observations
303 of deposition are probably not everywhere representative for a 1° or larger resolution and
304 observations of precipitation may also not be homogenous in all directions at that scale,
305 especially over heterogeneous terrain. So, for example, the coarse resolution of the model, even
306 with added measurements is likely not accurately capturing gradients between coastal and inland

Deleted: ·

Deleted: ·

309 deposition. While higher resolution precipitation values are available in some regions (e.g.,
310 PRISM in the US), there is still a dearth of both wet and dry deposition measurements. Even on
311 the North American continental scale, Schwede et al. (2011) showed that partially overlapping
312 dry deposition estimates from CASTNET (USA) and CAPMoN (Canada) can be very different,
313 despite using similar methodologies. This adds uncertainty to the dry deposition data (though
314 there are very few dry deposition estimates included in this study) and emphasizes the
315 importance of understanding deposition velocity model methodology.

316 The differences between the TDep, MMM, and MMF gridded deposition (Figure 5) are clearly
317 visible in the center of the US. While the general patterns of deposition are similar for the three
318 products, the magnitude of deposition in the aggregated TDep dataset ($1^\circ \times 1^\circ$) is higher in the
319 eastern US and lower in the western US than either of the other two deposition fields. This
320 difference is likely due to the precipitation dataset used to calculate wet deposition. The MMF
321 deposition is based on the MMM dataset; therefore, both utilize the same precipitation dataset,
322 from a combination of 11 global models. However, TDep wet deposition is produced by
323 multiplying PRISM precipitation data and an interpolated gridded surface dataset of wet NH_4^+
324 concentrations. PRISM is a reanalysis product designed to interpolate precipitation in
325 particularly complex landscapes using weather radar and rainfall gauge observations, though it is
326 not identical to observations because it used long-term averages as predictor grids (Zhang et al.,
327 2018). It captures much more localized variation in precipitation due to geographical variations
328 which are not captured in the lower resolution global precipitation models used in the HTAP II
329 MMM (Tan et al., 2018a). To illustrate this, we compare PRISM to the available Community
330 Atmosphere Model with Chemistry (<https://www2.acom.ucar.edu/gcm/cam-chem>, “CAM-
331 Chem”), which was one of the models in the HTAP II ensemble. Subtracting the CAM-Chem
332 precipitation output over the US from aggregated PRISM precipitation shows that CAM-Chem
333 greatly underestimates precipitation volume in the US in 2010 (Figure S6). We note, however,
334 that this comparison does not take differences in precipitation frequency between the model and
335 observations into account. This matters because if the difference in precipitation volume comes
336 from a few large magnitude storms, it will not influence the overall wet deposition values much.
337 This is a good example of the differences that occur when comparing global and regional climate
338 models and serves to emphasize the importance of resolving spatial and temporal scales. The

339 total deposition within the US borders is similar for the MMF, HTAP II, and aggregated TDep
340 gridded surfaces; however, the spatial distribution is different.

341 MMF and MMM deposition distributions are similar because MMF is based on HTAP II.
342 Likewise, the MMF results are similar to the TDep values at observation locations because,
343 despite the difference in precipitation, both utilize the same NADP/NTN measurements to
344 constrain the models. The key difference between MMF, when compared to MMM, is that
345 measurement locations are not centered in each $1^\circ \times 1^\circ$ grid cell; therefore, the center of each grid
346 cell (the value compared to the observation, by interpolation to the station location) will not
347 exactly equal the measured deposition but will instead be equal to the measurements weighted
348 proportionally to distance from the centroid. This means that the graphical comparison of Figure
349 6 is showing the actual measurement locations and 3 different model results with some
350 meaningful influence from measurements that are nonetheless unique values, except in the very
351 rare instance that the measurement corresponds exactly to the center of a grid cell. Figure 6
352 shows a stronger correlation for SO_4 than Figures S2 and S3 do for the nitrogen species. This
353 could be related to the relatively shorter timescales of NO_y and NH_x in the atmosphere. The
354 relatively coarse resolution of the global models cannot deal with these gradients, so the shorter
355 timescales are reflected in the observations which are therefore less representative for the larger
356 grid scales of the models.

357 TDep maps of North American nitrogen deposition created with Schwede and Lear's
358 methodology (2014), using IDW, are widely in use and freely available from the NADP. The
359 sensitivity analysis demonstrates that as the interpolation distance increases, the influence of the
360 observations on the HTAP II grid increases, smoothing some of the artifacts that can occur using
361 a small interpolation distance (Figures 6, S2, S3). In this respect it is worth mentioning that the
362 original TDep dataset for North America used a maximum distance of 30 km plus half the cell
363 size of PRISM (2.07 km). While it is not entirely clear how this distance was determined,
364 operational factors such as the station density and the grid size of the regional model are likely
365 important factors. In contrast, the maximum distances explored in this study are much larger (1° ,
366 2.5° , 5°) and are more adapted to the grid size of the current generation of global atmospheric
367 chemistry transport models, and considerations of transport distances of atmospheric
368 components. From our analysis there is no obvious better weighting distance that improves the
369 comparison with observations. An adaptive distance weighting that considers the expected

370 gradients between the observation point and the remote model grid could be explored as a way
371 forward.

372 However, there are strong limitations associated with using IDW (Sahu et al., 2010), and other
373 interpolation methods such as kriging or geographically weighted regression could provide
374 smoother surfaces with fewer artifacts. IDW is a fast and flexible interpolation method, but it
375 does not minimize error and can produce inaccurate results in regions with sparse measurements
376 and large sub-grid variability. This problem is relevant to much of the world. The lack of
377 measurement sites globally is a hindrance that can be alleviated by including information
378 obtained from satellite remote sensing (Walker et al., 2019). Future work should also investigate
379 methods such as machine learning techniques with spatial information to avoid these limitations.

380 These results from measurement-model fusion are important because previous methods on a
381 global scale have relied primarily on models (Vet et al., 2014; Tan et al., 2018a). They compare
382 their results with measurements, of course, in order to demonstrate the model capabilities but
383 they do not explicitly incorporate point measurements into the final product. Our results serve to
384 emphasize that global models are adequately simulating deposition (in terms of total deposition
385 budgets) but that the regional discrepancies between models and measurements can still be quite
386 large; and measurement-model fusion helps to ameliorate this without changing the fundamental
387 model parameters and processes that actually capture the overall deposition reasonably well.

388 **6. Conclusions**

389 Sulfur and nitrogen deposition remain a serious concern for human and ecosystem health. We
390 update the 2010 deposition budgets using measurement-model fusion to combine the broad
391 spatial coverage of a model with accurate in-situ measurements. The total nitrogen deposition
392 budget is recalculated to 114.50 Tg-N and the sulfur budget is recalculated to 88.91 Tg-N,
393 representing about a 1% and 6.5% increase, respectively, from the modelled values. This work
394 emphasizes the necessity of combining models with observations wherever possible, to better
395 capture regional patterns and to inform policy and decision-making. Future work to improve
396 measurement-model fusion should investigate more advanced MMF methods to avoid the
397 limitations associated with IDW such as surface artifacts and high error in regions with sparse
398 measurements. It could also incorporate satellite remote sensing derived concentrations to

399 improve model estimates where in-situ measurements are not available, but a careful error
400 analysis is needed to avoid spurious results.

401 **Author Contribution**

402 HR carried out the methods and analyzed the results. JSF and FD designed the project. HR
403 prepared the manuscript with contributions from JSF and FD. RL, KH, and HF provided data.

404 **Competing Interests**

405 The authors declare no competing interests.

406 **Code Availability**

407 Data analysis was done using ArcMap Desktop 10.8.1, ArcGIS Pro, and R (R Core Team, 2022).

408

409 **References**

- 410 Adon, M., Galy-Lacaux, C., Yoboué, V., Delon, C., Lacaux, J. P., Castera, P., Gardrat, E.,
411 Pienaar, J., Al Ourabi, H., Laouali, D., Diop, B., Sigha-Nkamdjou, L., Akpo, A., Tathy, J. P.,
412 Lavenu, F., and Mougin, E.: Long term measurements of sulfur dioxide, nitrogen dioxide,
413 ammonia, nitric acid and ozone in Africa using passive samplers, *Atmos. Chem. Phys.*, 10,
414 7467–7487, <https://doi.org/10.5194/acp-10-7467-2010>, 2010.
- 415 Anderson, D. M., Burkholder, J. M., Cochlan, W. P., Glibert, P. M., Gobler, C. J., Heil, C. A.,
416 Kudela, R. M., Parsons, M. L., Rensel, J. E. J., Townsend, D. W., Trainer, V. L., and Vargo, G.
417 A.: Harmful algal blooms and eutrophication: Examining linkages from selected coastal regions
418 of the United States, *Harmful Algae*, 8, 39–53, <https://doi.org/10.1016/j.hal.2008.08.017>, 2008.
- 419 Acid Deposition Monitoring Network in East Asia (EANET): <https://www.eanet.asia/>, last
420 access: 18 November 2021.
- 421 Bobbink, R., Hicks, K., Galloway, J., Spranger, T., Alkemade, R., Ashmore, M., Bustamante,
422 M., Cinderby, S., Davidson, E., Dentener, F., Emmett, B., Erismann, J.-W., Fenn, M., Gilliam, F.,
423 Nordin, A., Pardo, L., and Vries, W. D.: Global assessment of nitrogen deposition effects on
424 terrestrial plant diversity: a synthesis, *Ecological Applications*, 20, 30–59,
425 <https://doi.org/10.1890/08-1140.1>, 2010.
- 426 Bowman, W. D., Cleveland, C. C., Halada, L., Hreško, J., and Baron, J. S.: Negative impact of
427 nitrogen deposition on soil buffering capacity, *Nature Geoscience*, 1, 767–770,
428 <https://doi.org/10.1038/ngeo339>, 2008.
- 429 Clark, C. M., Bai, Y., Bowman, W. D., Cowles, J. M., Fenn, M. E., Gilliam, F. S., Phoenix, G.
430 K., Siddique, I., Stevens, C. J., Sverdrup, H. U., and Throop, H. L.: Nitrogen Deposition and
431 Terrestrial Biodiversity, in: *Encyclopedia of Biodiversity*, Elsevier, 519–536,
432 <https://doi.org/10.1016/B978-0-12-384719-5.00366-X>, 2013.
- 433 Dentener, F., Drevet, J., Lamarque, J. F., Bey, I., Eickhout, B., Fiore, A. M., Hauglustaine, D.,
434 Horowitz, L. W., Krol, M., Kulshrestha, U. C., Lawrence, M., Galy-Lacaux, C., Rast, S.,
435 Shindell, D., Stevenson, D., Noije, T. V., Atherton, C., Bell, N., Bergman, D., Butler, T., Cofala,
436 J., Collins, B., Doherty, R., Ellingsen, K., Galloway, J., Gauss, M., Montanaro, V., Müller, J. F.,
437 Pitari, G., Rodriguez, J., Sanderson, M., Solmon, F., Strahan, S., Schultz, M., Sudo, K., Szopa,
438 S., and Wild, O.: Nitrogen and sulfur deposition on regional and global scales: A multimodel
439 evaluation, *Global Biogeochemical Cycles*, 20, <https://doi.org/10.1029/2005GB002672>, 2006.
- 440 Dise, N. B. and Stevens, J.: Nitrogen deposition and reduction of terrestrial biodiversity:
441 Evidence from temperate grasslands, *Sci. China Ser. C.-Life Sci.*, 48, 720–728,
442 <https://doi.org/10.1007/BF03187112>, 2005.
- 443 Doney, S. C., Mahowald, N., Lima, I., Feely, R. A., Mackenzie, F. T., Lamarque, J.-F., and
444 Rasch, P. J.: Impact of anthropogenic atmospheric nitrogen and sulfur deposition on ocean
445 acidification and the inorganic carbon system, *PNAS*, 104, 14580–14585,
446 <https://doi.org/10.1073/pnas.0702218104>, 2007.

447 European Monitoring and Evaluation Programme (EMEP): <https://www.emep.int/>, last access: 18
448 November 2021.

449 Canadian Air and Precipitation Monitoring Network: [https://www.canada.ca/en/environment-](https://www.canada.ca/en/environment-climate-change/services/air-pollution/monitoring-networks-data/canadian-air-precipitation.html)
450 [climate-change/services/air-pollution/monitoring-networks-data/canadian-air-precipitation.html](https://www.canada.ca/en/environment-climate-change/services/air-pollution/monitoring-networks-data/canadian-air-precipitation.html),
451 last access: 18 November 2021.

452 Fu, J. S., Carmichael, G. R., Dentener, F., Aas, W., Andersson, C., Barrie, L. A., Cole, A., Galy-
453 Lacaux, C., Geddes, J., Itahashi, S., Kanakidou, M., Labrador, L., Paulot, F., Schwede, D., Tan,
454 J., and Vet, R.: Improving Estimates of Sulfur, Nitrogen, and Ozone Total Deposition through
455 Multi-Model and Measurement-Model Fusion Approaches, *Environ. Sci. Technol.*, 56, 2134–
456 2142, <https://doi.org/10.1021/acs.est.1c05929>, 2022.

457 Galy-Lacaux, C., Delon, C., Solmon, F., Adon, M., Yoboué, V., Mphepya, J., Pienaar, J. J.,
458 Diop, B., Sigha, L., Dungall, L., Akpo, A., Mougin, E., Gardrat, E., and Castera, P.: Dry and Wet
459 Atmospheric Nitrogen Deposition in West Central Africa, in: Nitrogen Deposition, Critical
460 Loads and Biodiversity, edited by: Sutton, M. A., Mason, K. E., Sheppard, L. J., Sverdrup, H.,
461 Haeuber, R., and Hicks, W. K., Springer Netherlands, Dordrecht, 83–91,
462 https://doi.org/10.1007/978-94-007-7939-6_10, 2014.

463 Geddes, J. A. and Martin, R. V.: Global deposition of total reactive nitrogen oxides from 1996 to
464 2014 constrained with satellite observations of NO₂ columns, *Atmospheric Chemistry and*
465 *Physics*, 17, 10071–10091, <https://doi.org/10.5194/acp-17-10071-2017>, 2017.

466 Heisler, J., Glibert, P. M., Burkholder, J. M., Anderson, D. M., Cochlan, W., Dennison, W. C.,
467 Dortch, Q., Gobler, C. J., Heil, C. A., Humphries, E., Lewitus, A., Magnien, R., Marshall, H. G.,
468 Sellner, K., Stockwell, D. A., Stoecker, D. K., and Suddleson, M.: Eutrophication and harmful
469 algal blooms: A scientific consensus, *Harmful Algae*, 8, 3–13,
470 <https://doi.org/10.1016/j.hal.2008.08.006>, 2008.

471 INDAAF – International Network to study Deposition and Atmospheric chemistry in Africa:
472 <https://indaaf.obs-mip.fr/>, last access: 18 November 2021.

473 Jia, Y., Yu, G., He, N., Zhan, X., Fang, H., Sheng, W., Zuo, Y., Zhang, D., and Wang, Q.:
474 Spatial and decadal variations in inorganic nitrogen wet deposition in China induced by human
475 activity, *Sci Rep*, 4, 3763, <https://doi.org/10.1038/srep03763>, 2014.

476 Kicklighter, D. W., Melillo, J. M., Monier, E., Sokolov, A. P., and Zhuang, Q.: Future nitrogen
477 availability and its effect on carbon sequestration in Northern Eurasia, *Nat Commun*, 10, 3024,
478 <https://doi.org/10.1038/s41467-019-10944-0>, 2019.

479 Labrador, L., Volosciuk, C., and Cole, A.: Measurement-Model Fusion for Global Total
480 Atmospheric Deposition, a WMO initiative, World Meteorological Organization, 2020.

481 Lamarque, J.-F., Dentener, F., McConnell, J., Ro, C.-U., Shaw, M., Vet, R., Bergmann, D.,
482 Cameron-Smith, P., Dalsoren, S., Doherty, R., Faluvegi, G., Ghan, S. J., Josse, B., Lee, Y. H.,
483 MacKenzie, I. A., Plummer, D., Shindell, D. T., Skeie, R. B., Stevenson, D. S., Strode, S., Zeng,
484 G., Curran, M., Dahl-Jensen, D., Das, S., Fritzsche, D., and Nolan, M.: Multi-model mean

485 nitrogen and sulfur deposition from the Atmospheric Chemistry and Climate Model
486 Intercomparison Project (ACCMIP): evaluation of historical and projected future changes,
487 *Atmos. Chem. Phys.*, 13, 7997–8018, <https://doi.org/10.5194/acp-13-7997-2013>, 2013.

488 Li, R., Cui, L., Zhao, Y., Zhang, Z., Sun, T., Li, J., Zhou, W., Meng, Y., Huang, K., and Fu, H.:
489 Wet deposition of inorganic ions in 320 cities across China: spatio-temporal variation, source
490 apportionment, and dominant factors, *Atmospheric Chemistry and Physics*, 19, 11043–11070,
491 <https://doi.org/10.5194/acp-19-11043-2019>, 2019.

492 Liu, L., Zhang, X., Xu, W., Liu, X., Zhang, Y., Li, Y., Wei, J., Lu, X., Wang, S., Zhang, W.,
493 Zhao, L., Wang, Z., and Wu, X.: Fall of oxidized while rise of reduced reactive nitrogen
494 deposition in China, *Journal of Cleaner Production*, 272, 122875,
495 <https://doi.org/10.1016/j.jclepro.2020.122875>, 2020.

496 Lu, Z., Streets, D. G., Zhang, Q., Wang, S., Carmichael, G. R., Cheng, Y. F., Wei, C., Chin, M.,
497 Diehl, T., and Tan, Q.: Sulfur dioxide emissions in China and sulfur trends in East Asia since
498 2000, *Atmos. Chem. Phys.*, 10, 6311–6331, <https://doi.org/10.5194/acp-10-6311-2010>, 2010.

499 Luo, X. S., Tang, A. H., Shi, K., Wu, L. H., Li, W. Q., Shi, W. Q., Shi, X. K., Erisman, J. W.,
500 Zhang, F. S., and Liu, X. J.: Chinese coastal seas are facing heavy atmospheric nitrogen
501 deposition, *Environ. Res. Lett.*, 9, 095007, <https://doi.org/10.1088/1748-9326/9/9/095007>, 2014.

502 National Atmospheric Deposition Program: <https://nadp.slh.wisc.edu/>, last access: 18 November
503 2021.

504 Qu, L., Xiao, H., Zheng, N., Zhang, Z., and Xu, Y.: Comparison of four methods for spatial
505 interpolation of estimated atmospheric nitrogen deposition in South China, *Environ Sci Pollut*
506 *Res*, 24, 2578–2588, <https://doi.org/10.1007/s11356-016-7995-0>, 2017.

507 R Core Team: *R: A Language and Environment for Statistical Computing*, 2022.

508 Sahu, S. K., Gelfand, A. E., and Holland, D. M.: Fusing point and areal level space–time data
509 with application to wet deposition, *Journal of the Royal Statistical Society: Series C (Applied*
510 *Statistics)*, 59, 77–103, <https://doi.org/10.1111/j.1467-9876.2009.00685.x>, 2010.

511 Schwede, D., Zhang, L., Vet, R., and Lear, G.: An intercomparison of the deposition models
512 used in the CASTNET and CAPMoN networks, *Atmospheric Environment*, 45, 1337–1346,
513 <https://doi.org/10.1016/j.atmosenv.2010.11.050>, 2011.

514 Schwede, D., Cole, A., Vet, R., and Lear, G.: Ongoing U.S. - Canada Collaboration on Nitrogen
515 and Sulfur Deposition, 5, 2019.

516 Schwede, D. B. and Lear, G. G.: A novel hybrid approach for estimating total deposition in the
517 United States, *Atmospheric Environment*, 92, 207–220,
518 <https://doi.org/10.1016/j.atmosenv.2014.04.008>, 2014.

519 Sirois, A.: The effects of missing data on the calculation of precipitation-weighted-mean
520 concentrations in wet deposition, *Atmospheric Environment. Part A. General Topics*, 24, 2277–
521 2288, [https://doi.org/10.1016/0960-1686\(90\)90321-D](https://doi.org/10.1016/0960-1686(90)90321-D), 1990.

522 Tan, J., Fu, J. S., Dentener, F., Sun, J., Emmons, L., Tilmes, S., Sudo, K., Flemming, J., Jonson,
523 J. E., Gravel, S., Bian, H., Davila, Y., Henze, D. K., Lund, M. T., Kucsera, T., Takemura, T., and
524 Keating, T.: Multi-model study of HTAP II on sulfur and nitrogen deposition, *Atmospheric
525 Chemistry and Physics*, 18, 6847–6866, <https://doi.org/10.5194/acp-18-6847-2018>, 2018a.

526 Tan, J., Fu, J. S., Dentener, F., Sun, J., Emmons, L., Tilmes, S., Flemming, J., Takemura, T.,
527 Bian, H., Zhu, Q., Yang, C.-E., and Keating, T.: Source contributions to sulfur and nitrogen
528 deposition – an HTAP II multi-model study on hemispheric transport, *Atmospheric Chemistry
529 and Physics*, 18, 12223–12240, <https://doi.org/10.5194/acp-18-12223-2018>, 2018b.

530 Tørseth, K., Aas, W., Breivik, K., Fjæraa, A. M., Fiebig, M., Hjellbrekke, A. G., Lund Myhre,
531 C., Solberg, S., and Yttri, K. E.: Introduction to the European Monitoring and Evaluation
532 Programme (EMEP) and observed atmospheric composition change during 1972 - 2009,
533 *Atmospheric Chemistry and Physics*, 12, 5447–5481, <https://doi.org/10.5194/acp-12-5447-2012>,
534 2012.

535 Clean Air Status and Trends Network (CASTNET): <https://www.epa.gov/castnet>, last access: 18
536 November 2021.

537 Vet, R., Artz, R. S., Carou, S., Shaw, M., Ro, C.-U., Aas, W., Baker, A., Bowersox, V. C.,
538 Dentener, F., Galy-Lacaux, C., Hou, A., Pienaar, J. J., Gillett, R., Forti, M. C., Gromov, S., Hara,
539 H., Khodzher, T., Mahowald, N. M., Nickovic, S., Rao, P. S. P., and Reid, N. W.: A global
540 assessment of precipitation chemistry and deposition of sulfur, nitrogen, sea salt, base cations,
541 organic acids, acidity and pH, and phosphorus, *Atmospheric Environment*, 93, 3–100,
542 <https://doi.org/10.1016/j.atmosenv.2013.10.060>, 2014.

543 de Vries, W., Solberg, S., Dobbertin, M., Sterba, H., Laubhann, D., van Oijen, M., Evans, C.,
544 Gundersen, P., Kros, J., Wamelink, G. W. W., Reinds, G. J., and Sutton, M. A.: The impact of
545 nitrogen deposition on carbon sequestration by European forests and heathlands, *Forest Ecology
546 and Management*, 258, 1814–1823, <https://doi.org/10.1016/j.foreco.2009.02.034>, 2009.

547 Walker, J. T., Beachley, G., Amos, H. M., Baron, J. S., Bash, J., Baumgardner, R., Bell, M. D.,
548 Benedict, K. B., Chen, X., Clow, D. W., Cole, A., Coughlin, J. G., Cruz, K., Daly, R. W.,
549 Decina, S. M., Elliott, E. M., Fenn, M. E., Ganzeveld, L., Gebhart, K., Isil, S. S., Kerschner, B.
550 M., Larson, R. S., Lavery, T., Lear, G. G., Macy, T., Mast, M. A., Mishoe, K., Morris, K. H.,
551 Padgett, P. E., Pouyat, R. V., Puchalski, M., Pye, H. O. T., Rea, A. W., Rhodes, M. F., Rogers,
552 C. M., Saylor, R., Scheffe, R., Schichtel, B. A., Schwede, D. B., Sexstone, G. A., Sive, B. C.,
553 Sosa Echeverría, R., Templer, P. H., Thompson, T., Tong, D., Wetherbee, G. A., Whitlow, T. H.,
554 Wu, Z., Yu, Z., and Zhang, L.: Toward the improvement of total nitrogen deposition budgets in
555 the United States, *Science of The Total Environment*, 691, 1328–1352,
556 <https://doi.org/10.1016/j.scitotenv.2019.07.058>, 2019.

557 Wen, Z., Xu, W., Li, Q., Han, M., Tang, A., Zhang, Y., Luo, X., Shen, J., Wang, W., Li, K., Pan,
558 Y., Zhang, L., Li, W., Collett, J. L., Zhong, B., Wang, X., Goulding, K., Zhang, F., and Liu, X.:

559 Changes of nitrogen deposition in China from 1980 to 2018, *Environment International*, 144,
560 106022, <https://doi.org/10.1016/j.envint.2020.106022>, 2020.

561 Xu, W., Luo, X. S., Pan, Y. P., Zhang, L., Tang, A. H., Shen, J. L., Zhang, Y., Li, K. H., Wu, Q.
562 H., Yang, D. W., Zhang, Y. Y., Xue, J., Li, W. Q., Li, Q. Q., Tang, L., Lu, S. H., Liang, T.,
563 Tong, Y. A., Liu, P., Zhang, Q., Xiong, Z. Q., Shi, X. J., Wu, L. H., Shi, W. Q., Tian, K., Zhong,
564 X. H., Shi, K., Tang, Q. Y., Zhang, L. J., Huang, J. L., He, C. E., Kuang, F. H., Zhu, B., Liu, H.,
565 Jin, X., Xin, Y. J., Shi, X. K., Du, E. Z., Dore, A. J., Tang, S., Collett, J. L., Goulding, K., Sun,
566 Y. X., Ren, J., Zhang, F. S., and Liu, X. J.: Quantifying atmospheric nitrogen deposition through
567 a nationwide monitoring network across China, *Atmos. Chem. Phys.*, 15, 12345–12360,
568 <https://doi.org/10.5194/acp-15-12345-2015>, 2015.

569 Xu, W., Zhang, L., and Liu, X.: A database of atmospheric nitrogen concentration and deposition
570 from the nationwide monitoring network in China, *Sci Data*, 6, 51,
571 <https://doi.org/10.1038/s41597-019-0061-2>, 2019.

572 Zhang, M., Leon, C. de, and Migliaccio, K.: Evaluation and comparison of interpolated gauge
573 rainfall data and gridded rainfall data in Florida, USA, *Hydrological Sciences Journal*, 63, 561–
574 582, <https://doi.org/10.1080/02626667.2018.1444767>, 2018.

575 Zhang, Y., Foley, K. M., Schwede, D. B., Bash, J. O., Pinto, J. P., and Dennis, R. L.: A
576 Measurement-Model Fusion Approach for Improved Wet Deposition Maps and Trends, *Journal*
577 *of Geophysical Research: Atmospheres*, 124, 4237–4251,
578 <https://doi.org/10.1029/2018JD029051>, 2019.

579 Zhao, Y., Zhang, L., Chen, Y., Liu, X., Xu, W., Pan, Y., and Duan, L.: Atmospheric nitrogen
580 deposition to China: A model analysis on nitrogen budget and critical load exceedance,
581 *Atmospheric Environment*, 153, 32–40, <https://doi.org/10.1016/j.atmosenv.2017.01.018>, 2017.

582 Zhu, J., Chen, Z., Wang, Q., Xu, L., He, N., Jia, Y., Zhang, Q., and Yu, G.: Potential transition in
583 the effects of atmospheric nitrogen deposition in China, *Environmental Pollution*, 258, 113739,
584 <https://doi.org/10.1016/j.envpol.2019.113739>, 2020.

585